Optik - International Journal for Light and Electron Optics 185 (2019) 1261–1269

Contents lists available at ScienceDirect

Optik

journal homepage: www.elsevier.com/locate/ijleo

Original research article

One- and two-photon-induced magneto-optical properties of hyperbolic-type quantum wells

Nguyen D. Hien[a,b], Doan V. Thuan[c,*], C.A. Duque[d], E. Feddi[e], F. Dujardin[f], Le T.T. Phuong[g], Bui D. Hoi[g], Chuong V. Nguyen[h], Le T.N. Tu[i], Huynh V. Phuc[i], Nguyen N. Hieu[j,*]

[a] Laboratory of Magnetism and Magnetic Materials, Advanced Institute of Materials Science, Ton Duc Thang University, Ho Chi Minh City, Viet Nam
[b] Faculty of Applied Sciences, Ton Duc Thang University, Ho Chi Minh City, Viet Nam
[c] NTT Hi-Tech Institute, Nguyen Tat Thanh University, Ho Chi Minh City, Viet Nam
[d] Grupo de Materia Condensada-UdeA, Instituto de Física, Facultad de Ciencias Exactas y Naturales, Universidad de Antioquia UdeA, Calle 70 No. 52-21, Medellín, Colombia
[e] LaMCScI, Group of Optoelectronic of Semiconductors and Nanomaterials, ENSET, Mohammed V University in Rabat, Rabat, Morocco
[f] Université de Lorraine, LCP-A2MC, 57000 Metz, France
[g] Physics Department, University of Education, Hue University, Hue 530000, Viet Nam
[h] Department of Materials Science and Engineering, Le Quy Don Technical University, Ha Noi 100000, Viet Nam
[i] Division of Theoretical Physics, Dong Thap University, Cao Lanh 870000, Viet Nam
[j] Institute of Research and Development, Duy Tan University, Da Nang 550000, Viet Nam

ARTICLE INFO

Keywords:
Magneto-optical properties
Two-photon absorption
Al-concentration
Hydrostatic pressure
Temperature

ABSTRACT

We investigate the combined effects of hydrostatic pressure, Al-concentration, temperature, and well-width parameter on the magneto-optical absorption properties (MOAPs) of a hyperbolic-type quantum well (HTQW). The results covered all possible processes: both phonon absorption and emission as well as both one- and two-photon. Our results show that the MOAPs of the HTQW significantly depend on the pressure, the Al-concentration, the temperature, and the well-width. We also suggest two new expressions for the dependence of the full-width at half-maximum on the pressure and concentration which need an experimental study to evaluate their validity. Our study provides a systematic results of the combined effects of pressure, Al-concentration, temperature, electron-phonon scattering, and the two-photon absorption on the nonlinear optical properties of such two-dimensional semiconductors, which would be useful for the applications in photonic devices.

1. Introduction

Nonlinear optical absorption properties (NOAP) of low-dimensional systems, including the magneto-optical absorption properties (MOAPs), are the most widely studied phenomena over the past few decades. Interest in NOAP originates in their potential applications in electro-optical modulators [1], from mid-infrared to the submillimeter laser amplifiers [2], and infrared photo-detectors [3,4]. The nonlinear magneto-optical response is demonstrated to be strongly influenced by the quantum well states [5]. The optical absorption coefficients (OAC) and refractive index changes (RIC) have been studied in wide range such as in spherical quantum dots [6,7], spherical dome shells [8], quantum rings [9], double quantum wells [10], cylindrical quantum well wire [11], and quantum

* Corresponding authors.
E-mail addresses: nguyendinhhien@tdtu.edu.vn (N.D. Hien), dvthuan@ntt.edu.vn (D.V. Thuan), hieunn@duytan.edu.vn (N.N. Hieu).

https://doi.org/10.1016/j.ijleo.2019.03.151
Received 19 January 2019; Received in revised form 12 March 2019; Accepted 26 March 2019
0030-4026/ © 2019 Elsevier GmbH. All rights reserved.

wells [12–14]. Results show that the OAC and the RIC in these semiconductor systems significantly depend on the geometric structure of the system, the temperature, and the applied external electric and magnetic fields.

The two-photon absorption (2PA) is one unique type of the nonlinear processes. Since 2PA measurements can provide new information on the electronic states in semiconducting materials [15], study about the 2PA helps us to deeply understand the nature of nonlinear processes in both theory and experiment [16]. That is the reason why it is one of the most attractive subjects in recent years. Shimizu et al. [17] developed a general theory for 2PA spectra, which can be applied for semiconductors with an arbitrary dimension. Recently, when calculating the 2PA transition energy and oscillator strength in PbS quantum dots (QDs) Padilha et al. [18] demonstrated that the 2PA process increases with increasing quantum confinement because of the special band structure of PbS. The 2PA induced photoluminescence in $CsPbBr_3$ QDs has also been investigated at a wide range of temperature [19]. Spector [20] presented theoretical of 2PA for quasi-one and two-dimensional quantum-well structures and found that the absorption coefficient in these systems is larger than that in the bulk materials. The 2PA is also widely investigated in QDs with different materials [21–25] and in quantum wells [26]. In a previous work [27], we investigated the MOAPs in a hyperbolic-type quantum well (HTQW) excited by the 2PA process. The effects of temperature, magnetic field, and the well-width on the magneto-optical absorption coefficient (MOAC) and the full-width at half-maximum (FWHM) were studied. However, how the combined effects of the pressure, temperature, and Al-concentration on the MOAC and the FWHM in HTQW perform still remains unclear.

Because of their direct influence on the basic parameters in GaAs/GaAlAs low-dimensional systems such as the confining potential [28–30], the electron effective mass [31–33], the dielectric constants [34–39], and the $\Gamma - X$ mixing phenomenon [31,40–42], the combined effects of hydrostatic pressure, Al-concentration, and temperature directly affect the electronic and therefore the optical properties. The hydrostatic pressure dependent OAC and RIC in a quantum well with different well-shapes have been studied by Ozturk and Sökmen [28]. Welber et al. [29] investigated the effect of these parameters on the direct energy gap of GaAs semiconductor. A combined effect of these parameters on the g-factor [31,32] in quantum wells has also been investigated. For the optical properties, a simultaneous effect of the pressure, the concentration, and the temperature on the linear and nonlinear OACs has been studied widely in quantum rings [9,33], in QDs [36,43], and in quantum wells [38,44–46]. However, these combined effects on the nonlinear MOAPs of the HTQW are still open.

In this work, we will focus on the combined-effect of these parameters on the linear and nonlinear MOAPs of an HTQW. The 2PA and the electron-longitude optical (LO) phonon scattering have been taken into account. The MOAPs are studied via surveying the MOAC and the FWHM. Our study provides a systematic result of the combined effects of hydrostatic pressure, Al-concentration, temperature, electron–phonon scattering, and the 2PA process on the optical properties of such two-dimensional semiconductors.

2. Theoretical framework

2.1. Basic formalism

We start with the Al-concentration (s), hydrostatic pressure (P), and temperature (T) dependent confining potential in the z-direction of a GaAs/$Ga_{1-s}Al_sAs$ HTQW, which is given as follows [47,48]

$$U(z, s, P, T) = U_0(s, P, T)\left(\frac{\eta}{z} - \frac{z}{\eta}\right)^2, \tag{1}$$

where η is a parameter controlling the well-width, s is the Al-concentration in the barrier material, and [28–30]

$$U_0(s, P, T) = Q_c \begin{cases} U_{01}(s, P, T), & P \le P_1 \\ U_{02}(s, P, T), & P_1 < P \le P_2. \end{cases} \tag{2}$$

Here $Q_c = 0.6$ is the fraction of the band gap discontinuity [31], and

$$U_{01}(s, P, T) = E_g^{\Gamma}(s, P, T) - E_g^{\Gamma}(0, P, T), \tag{3}$$

$$U_{02}(s, P, T) = E_g^{X}(s, P, T) - E_g^{\Gamma}(0, P, T) + S_0\, s[P - P_1(s, T)]/P. \tag{4}$$

In this equation, $E_g^i(s, P, T)$ is the conduction band energy gap function at i-point ($i = \Gamma, X$), which is read as follows

$$E_g^i(s, P, T) = a_i + b_i s + c_i s^2 + d_i P - \frac{e_i T^2}{f_i + T}, \tag{5}$$

where the values of these parameters are listed in Table 1 of Ref. [45]. The quantity $S_0 = 250$ meV is a fitted parameter [40]. The quantities $P_1 = P_1(s, T)$ and $P_2 = P_2(s, T)$, respectively, are the cross-over pressure between $E_g^X(s, P, T)$ and $E_g^{\Gamma}(s, P, T)$ and between $E_g^X(s, P, T)$ and $E_g^{\Gamma}(0, P, T)$. For example, at $s = 0.3$ and $T = 77$ K, the corresponding values of $P_1(s, T)$ and $P_2(s, T)$ are 9.1 kbar and 44.6 kbar, respectively.

In the effective mass approximation, the Hamiltonian of an electron in an HTQW under the above-cited parameters and in the presence of a uniform magnetic field $\mathbf{B} = (0, 0, B)$ is given by

$$\mathcal{H} = \frac{(\mathbf{p} + e\mathbf{A})^2}{2m^*(s, P, T)} + U(z, s, P, T), \tag{6}$$

where **p** and e are, respectively, the momentum operator and the absolute charge of a conduction electron, and $\mathbf{A} = (0, Bx, 0)$ is the vector potential in the symmetric gauge. The expression of P- and T-dependent electron effective mass $m^*(s, P, T)$ is given as follows [31–33]

$$\frac{m_e}{m^*(s, P, T)} = \frac{\Lambda(s)}{3}\left[\frac{2}{E_g^{\Gamma}(s, P, T)} + \frac{1}{E_g^{\Gamma}(s, P, T) + \Delta(s)}\right] + 1 + \delta(s), \tag{7}$$

where m_e being the free electron mass, $\Lambda(s) = (28900 - 6290s)$ meV is the inter-band matrix element, $\Delta(s) = (341 - 66s)$ meV is the valence-band spin-orbit splitting, and $\delta(s) = -3.935 + 0.488s + 4.938s^2$ is a parameter associated with the remote-band effects. The electron eigenfunctions and eigenvalues are [49]

$$|\lambda\rangle = |N, n, k_y\rangle = \frac{e^{ik_y y}}{\sqrt{L_y}}\psi_N(x - x_0)\xi_n(z), \tag{8}$$

$$E_\lambda \equiv E_{N,n} = \left(N + \frac{1}{2}\right)\hbar\omega_c + \varepsilon_n, \quad N = 0, 1, 2, ... \tag{9}$$

Here, N denotes the Landau level (LL)-index, $\psi_N(x - x_0)$ is the Nth normalized harmonic-oscillator function centered at $x_0 = -\alpha_c^2 k_y$ with $\alpha_c = [\hbar/m^*(s, P, T)\omega_c]^{1/2}$ being the magnetic length and $\omega_c = eB/m^*(s, P, T)$; k_y and L_y are the y-direction electron wave vector and normalized length, respectively. The components of the wave-functions in the z-direction and the eigenvalues are [47,48]

$$\xi_n(z) = A_n z^{\alpha+1/2} e^{-\beta z^2} {}_1F_1(-n, \alpha + 1, 2\beta z^2), \tag{10}$$

$$\varepsilon_n = \frac{2\hbar}{\eta}\sqrt{\frac{2U_0(s, P, T)}{m^*(s, P, T)}}\left(n + \frac{1}{2} + \frac{\alpha}{2} - \eta^2\beta\right), \tag{11}$$

where $n = 0, 1, 2, \ldots$, is the electronic subband index, $\beta = [m^*(s, P, T)U_0(s, P, T)/2\hbar^2\eta^2]^{1/2}$ which has the unit of m^{-2}, $\alpha = (16\eta^4\beta^2 + 1)^{1/2}/2$ being a dimensionless quantity, and ${}_1F_1$ refer to the confluent hypergeometric functions. $A_0 = 2^{\alpha/2+1}\beta^{(\alpha+1)/2}/(\Gamma(\alpha + 1))^{1/2}$ and $A_1 = A_0(\alpha + 1)^{1/2}$ are the normalization constants for the two first states.

2.2. The magneto-optical absorption coefficient

In order to study the MOAPs of the HTQW, one needs to have the expression of the MOAC, which is expressed as [50]

$$K(\Omega) = \frac{1}{V_0(I_0/\hbar\Omega)}\sum_{\lambda,\lambda''}\mathcal{W}^{\pm}_{\lambda'',\lambda} f_\lambda(1 - f_{\lambda''}), \tag{12}$$

where V_0 is the volume of the system, I_0 is the optical intensity, $\hbar\Omega$ is the photon energy, and $f_\lambda = f_{N,n}$ ($f_{\lambda''} = f_{N'',n''}$) is the electron distribution function for the initial (final) state. The transition matrix element per unit area for the three particles interaction (electron, photon, phonon) is given as follows by the Born's second-order golden rule [51], including the k-photon absorption process [52,53]

$$\begin{aligned}\mathcal{W}^{\pm}_{\lambda'',\lambda} = & \frac{2\pi}{\hbar}\sum_{\lambda',\mathbf{q}}\sum_{k=1}^{\infty}(|\mathcal{M}^{\pm}_{\lambda'',\lambda'}|^2|\mathcal{M}^{\mathrm{rad}}_{\lambda',\lambda}|^2/\hbar^2\Omega^2) \\ & \times\frac{(\alpha_0 q)^{2k}}{(k!)^2 2^{2k}}\delta(E_{\lambda''} - E_\lambda - k\hbar\Omega \pm \hbar\omega_0),\end{aligned} \tag{13}$$

where λ' is an intermediate/virtual state, the upper (plus) and lower (minus) signs stand for, respectively, the emission and absorption of a LO-phonon of wave vector $\mathbf{q} = (q_\perp, q_z)$ and of energy $\hbar\omega_0$, and α_0 is the dressing parameter. Eq. (13) describes the transition of an electron between the initial state λ and the final state λ'' occurring first by absorption k-photons of energy $\hbar\Omega$ to transfer from state λ to state λ' and then the subsequent absorption (minus sign) or emission (plus sign) of a LO-phonon of energy $\hbar\omega_0$ to transfer to state λ''.

The matrix element for the electron-phonon scattering is expressed by [54]

$$|\mathcal{M}^{\pm}_{\lambda'',\lambda'}|^2 = |V(q)|^2|\mathcal{F}_{n'',n'}(\pm q_z)|^2|J_{N'',N'}(q_\perp)|^2 N_0^{\pm}\delta_{k''_y,k'_y\pm q_y}, \tag{14}$$

where

$$|V(q)|^2 = \frac{4\pi e^2\hbar\omega_0}{\varepsilon_0\chi^* V_0 q^2}, \tag{15}$$

$$\mathcal{F}_{n'',n'}(\pm q_z) = \int_0^\infty e^{\pm iq_z z}\xi^*_{n''}(z)\xi_{n'}(z)\mathrm{d}z, \tag{16}$$

$$|J_{N'',N'}(q_\perp)|^2 = \frac{N'!}{N''!}e^{-u}u^{N''-N'}L_{N'}^{N''-N'}(u), \tag{17}$$

with $u = \alpha_c^2 q_\perp^2/2$ and $L_{N'}^{N''-N'}(u)$ being the associated Laguerre polynomials where $N'' \geq N'$, and ϵ_0 is the permittivity of the vacuum. The quantity $\chi^*(s, P, T)$ is defined as follows

$$\frac{1}{\chi^*(s, P, T)} = \frac{1}{\chi_\infty(s, P, T)} - \frac{1}{\chi_0(s, P, T)}, \tag{18}$$

where $\chi_\infty(s, P, T)$ and $\chi_0(s, P, T)$ are the P-, s-, and T-dependent high- and low-frequency dielectric constants, respectively. They are given by $\chi_\infty(s, P, T) = 10.89 - 2.73s$ and $\chi_0(s, P, T) = \chi_0(0, P, T) - 3.12s$ [34,35], where the P- and T-dependent low-frequency dielectric constant is [36–39]

$$\chi_0(0, P, T) = \begin{cases} \sigma_1 \exp[-\mu P + \nu_1(T - T_1)], & T < 200\,\mathrm{K}, \\ \sigma_2 \exp[-\mu P + \nu_2(T - T_2)], & T \geq 200\,\mathrm{K}, \end{cases} \tag{19}$$

with $\sigma_1 = 12.47$, $\sigma_2 = 13.18$, $\mu = 1.73 \times 10^{-3}\,\mathrm{kbar}^{-1}$, $\nu_1 = 9.4 \times 10^{-5}\,\mathrm{K}^{-1}$, $\nu_2 = 20.4 \times 10^{-5}\,\mathrm{K}^{-1}$, $T_1 = 75.6\,\mathrm{K}$, and $T_2 = 300\,\mathrm{K}$.

The matrix element for electron-photon interaction is [55]

$$|\mathcal{M}_{\lambda',\lambda}^{\mathrm{rad}}|^2 = \frac{\Omega^2 A_0^2}{4} |\mathbf{n}\cdot e\mathcal{B}_{\lambda',\lambda}|^2, \tag{20}$$

where $\mathbf{n}$ is the polarized vector of the electromagnetic radiation, which is assumed to be linearly polarized along the x-axis, and $\mathcal{B}_{\lambda',\lambda} = \langle\lambda'|\mathbf{r}|\lambda\rangle$, with $\mathbf{r}$ being the position vector.

After making the necessary calculations we obtain the following expression for the MOAC

$$K(\Omega) = \sum_{N,n} \sum_{N'',n''} \sum_{N',n'} D(\mathcal{P}_1 + \mathcal{P}_2), \tag{21}$$

$$D = \frac{S^2 \chi^* e^4 \alpha_0^2 \hbar\omega_0}{32\pi^2\, \mathrm{cn}_0 \varepsilon_0^2 V_0 \alpha_c^6 \hbar^2 \Omega} |\mathcal{B}_{\lambda'\lambda}|^2 \mathrm{I}_{n'',n} f_{N,n}(1 - f_{N'',n''}), \tag{22}$$

$$I_{n'',n'} = \int_{-\infty}^{+\infty} |\mathcal{F}_{n'',n'}(\pm q_z)|^2 \mathrm{d}q_z, \tag{23}$$

$$\mathcal{P}_1 = N_\omega^- \delta(Q_1^-) + N_\omega^+ \delta(Q_1^+), \tag{24}$$

$$\mathcal{P}_2 = \frac{\alpha_0^2}{8\alpha_c^2}(N' + N'' + 1)[N_\omega^- \delta(Q_2^-) + N_\omega^+ \delta(Q_2^+)], \tag{25}$$

$$Q_k^\pm = \Delta E \pm \hbar\omega_0 - k\hbar\Omega, \tag{26}$$

with c being the speed of light, n_0 being the refractive index, $\Delta E = E_{N'',n''} - E_{N,n}$ being the energy separation, and $N_\omega^\pm = N_\omega + 0.5 \pm 0.5$ with $N_\omega = [e^{\hbar\omega_0/k_B T} - 1]^{-1}$ being the Bose distribution function in which $\hbar\omega_0 = (36.25 + 1.83s + 17.12s^2 - 5.11s^3)$ meV is the LO-phonon energy [34].

3. Discussion of results

For the numerical evaluation, we use the following characteristics: $n_e = 3 \times 10^{16}\,\mathrm{cm}^{-3}$, $n_0 = 3.2$, $\alpha_0 = 7.5\,\mathrm{nm}$, and $B = 10\,\mathrm{T}$ [27,34,44,56]. The following results are calculated in the extreme quantum limit, i.e., we only study the transition from the initial state with $N = 0$ and $n = 0$ to the final state with $N'' = 1$ and $n'' = 1$.

Fig. 1(a) shows the energy separation as a function of hydrostatic pressure for two distinct values of the Al-concentration, the temperature, and the η-well-width parameter. The solid (black) curve is plotted at $s = 0.3$, $T = 77\,\mathrm{K}$, and $\eta = 10\,\mathrm{nm}$, while for the other curves, there is only one quantity changed in compared to the solid one. For example, for the dashed (blue) curve, only the temperature is changed to $T = 300\,\mathrm{K}$ while all other parameters are kept fixed. The energy separation is shown as a decreasing function of the pressure but with different rates: the energy separation lessens gradually in the range of $P < P_1$ and then ΔE quickly drops when the pressure passes over the folding point P_1 and keeps decreasing. This behavior of the ΔE is in agreement with that reported in quantum rings [33] as well as in quantum wells [28,45], and can be explained as follows. We can see from Eq. (9) including Eq. (11) that the energy separation depends on the pressure through the confining potential $U_0(s, P, T)$ and the electron effective mass $m^*(s, P, T)$. In the range of $P < P_1$, the confining potential is unchanged. Therefore, for the given parameters, the reduction with pressure of energy separation is mainly the result of effective mass increasing. In the range of $P_1 < P \leq P_2$, the increase of the electron effective mass still keeps reducing the energy separation, but the ΔE is now additionally dropped by the reduction of the confining potential when the pressure increases. Consequently, the energy separation drops quickly with the pressure. Besides, the discontinuity of the energy separation comes from the discontinuity of the confining potential $U_0(s, P, T)$ with the pressure (see Eq. (2)). The interrupt point occurs at $P = P_1(s, T)$ which is independent from the η-parameter but shifts to the higher pressure region with the increase of the temperature and with the decrease of the concentration. In addition, we also see from Fig. 1(a) that the energy separation rises with temperature but reduces with η-parameter. The enhancement of the ΔE with Al-concentration is shown more clearly in Fig. 1(b).

The variation of the energy separation as functions of the concentration, s, for two fixed values of T, η, P is shown in Fig. 1(b). We

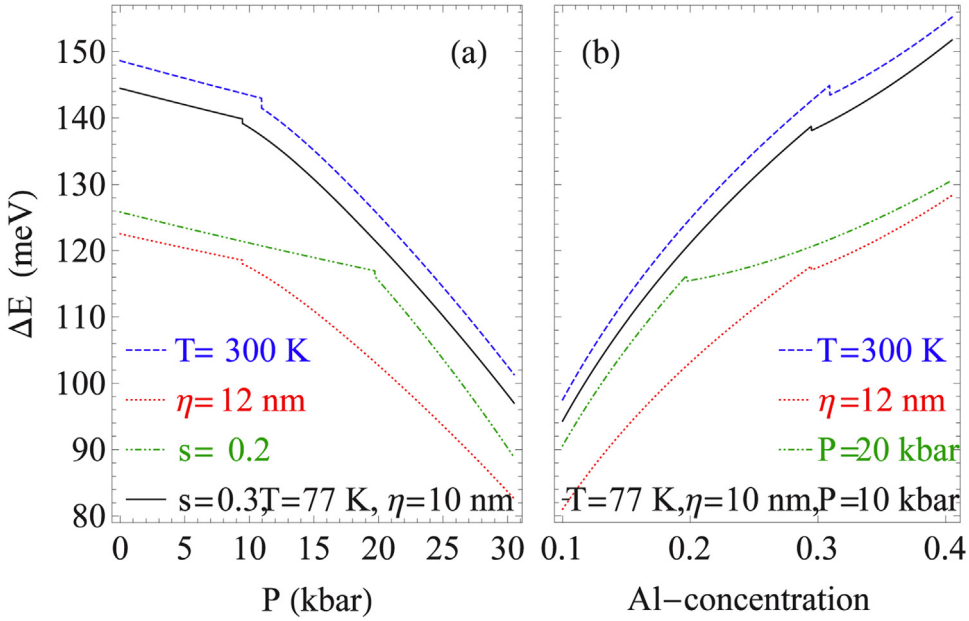

Fig. 1. Hydrostatic pressure (a) and Al-concentration (b) dependence of energy separation, ΔE. In each panel four setups of the parameters have been considered.

can see that the energy separation increases nonlinearly with Al-concentration, which is opposite to that in quantum rings [33] and in quantum wells [46,57], but is in agreement with that in other types of quantum wells [28,45]. With the increase of Al-concentration, there is a rivalry between the two processes: the enhancement of electron effective mass $m^*(s, P, T)$ leads to the decrease of energy separation, while the increase of confining potential $U_0(s, P, T)$ results in the increase of the ΔE. This result reveals that the effect of the increase of confinement potential on the behavior of the energy separation is dominant in comparison with the effect of the decrease of the electron effective mass.

Fig. 2(a) shows the $\hbar\Omega$-dependence of the MOAC for three different values of pressure. Four resonant peaks in each curve are labeled consecutively from "(1)" to "(4)" for P = 10 kbar (black solid curve), for example. These peaks are generated by the resonant

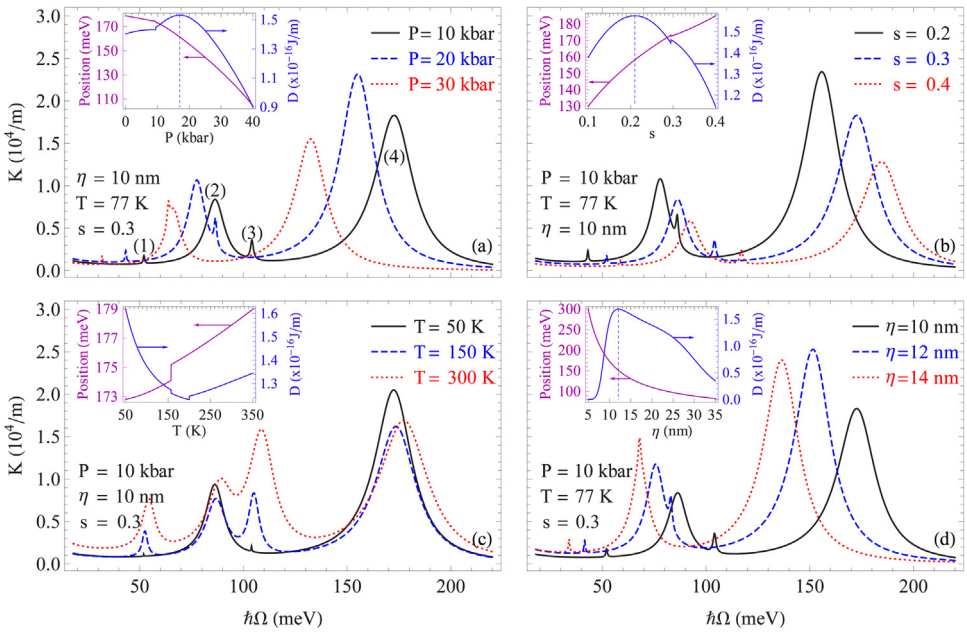

Fig. 2. Photon energy dependence of the MOAC for different values of hydrostatic pressure (a), Al-concentration (b), temperature (c), and η-parameter (d). The inset shows the P-dependencies of the higher-energy-peak position (the peak labeled by (4) in black curve) and the factor D (right vertical axis).

transition of electrons between the initial state and the final state by absorbing one- ($k = 1$) or two-photon ($k = 2$) followed by the absorption or the emission of one LO-phonon, which satisfies the resonance conditions

$$k\hbar\Omega = \Delta E \pm \hbar\omega_0, \quad k = 1, 2. \tag{27}$$

In Fig. 2(a), the peaks "(1)" and "(3)" describe the phonon absorption [corresponding the minus sign in Eq. (27)] while the peaks "(2)" and "(4)" describe the phonon emission [corresponding the plus sign in Eq. (27)]. The intensities of peaks "(2)" and "(4)" are much more than those of peaks "(1)" and "(3)". This implies that the phonon emission process is dominant in comparison with the phonon absorption. Besides, the result also reveals that the intensities due to the 2PA process (peaks "(1)" and "(3)") are smaller but comparable to those of the one-photon ones (peaks "(2)" and "(4)"). The values of the 2PA-peaks (in the case of $P = 10$ kbar, for example) are about 46% and 50% of those of the one-photon peaks for the phonon emission and the phonon absorption, respectively. These rates are equivalent to those reported in a special symmetric quantum well [58], which suggest that the 2PA process has a significant contribution to the total process and should not be ignored in inquiring the optical properties of such two-dimensional quantum wells.

For the influence of the hydrostatic pressure on the MOAC, we can see from Fig. 2(a) that the raise of pressure pushes the peak positions to the lower energy region (red-shift) and makes the change in peak values. The red-shift behavior is clearly illustrated in the inset, which shows that the peak positions reduce with the increasing pressure. Note that the peak positions are determined by Eq. (27). Because the phonon energy is independent from the pressure, the effect of pressure on the peak positions is totally through the energy separation ΔE. Therefore, the red-shift behavior is the result of the reducing ΔE when the pressure increases as shown in Fig. 1(a). This result is in good agreement with that reported in a square quantum well [45]. Now we turn our attention to discuss the influence of the pressure on the peak values. We can see that the pressure dependence of the peak values is non-monotonic, which results from the dependence of the factor D on the pressure as shown clearly in the inset. With the increase of pressure, the D-factor first increases, reaches its maximum at $P = 17.03$ kbar, and then begins to drop quickly with increasing pressure.

In Fig. 2(b) we show the $\hbar\Omega$-dependent MOAC for different values of s-parameter. The result shows that with the increase of Al-concentration the MOAC reduces in the intensity and shifts their peak positions to the higher energy side (blue-shift), agreeing with previous study [45]. We can see from Eq. (27) that the peak positions are determined by the energy separation and the phonon energy. Since both the ΔE and $\hbar\omega_0$ increase with the concentration, the blue-shift behavior of the peaks due to phonon absorption is clear. For the peaks due to phonon emission, there is a competition between ΔE and $\hbar\omega_0$ when the concentration increases. The blue-shift behavior of these peaks reveals that the increase of the energy separation is dominant in comparison with that of the LO-phonon energy. For the peaks intensity, note that the peaks intensity is proportional with the factor D. It can be seen from the inset that when the concentration increases, the factor D increases first, reaches its maximum value at $s = 0.21$ and then begins to decrease with increasing concentration. This result explains the reduction of the peaks value when the concentration increases from $s = 0.2$ to 0.4 as shown in Fig. 2(b).

To study the temperature influence on magneto-optical properties of the HTQW, in Fig. 2(c) we show the $\hbar\Omega$ dependent MOAC for different values of T. Unlike in previous work [27], in the present work, the temperature affects either the peak positions or the peak values. It is seen that when the temperature increases a slight blue-shift in the position is found but the change of the peak intensity due to phonon emission is non-monotonic. The peak intensity first decreases, reaching its minimum value at $T = 200$ K, and then begins to bounce increasing with the increase in temperature. The slight blue-shift behavior is cause of the slight increase of the ΔE with temperature [see Fig. 1(a) and (b)]. Meanwhile, the change peak intensity is illustrated by the change of D-factor with the temperature as shown in the inset. In addition, in comparison with the phonon emission peaks, the temperature effect on the phonon absorption ones is much stronger, which is consistent with previous works [27,58].

In Fig. 2(d), we show the $\hbar\Omega$-dependent MOAC for different values of η-parameter. The result showed that when the value of the η-parameter is large the MOAC peaks shift to the lower energies region and their intensities show a non-monotonic behavior: first increase and then decrease with the η-parameter. The red-shift trend results from the decrease of the ΔE with the η-parameter as shown in Fig. 1(a) and (b). This trend is also clearly illustrated in the inset where a reduction behavior of the peak positions with the increase of the η-parameter is observed. Meanwhile, since the peak intensities are associated with the D-factor. It is seen from the inset that when the η-parameter increase the D-factor first increases, reaching its maximum values at $\eta = 12.09$ nm, and then reduces with the further increase of η. This feature of the peak intensities is different from that reported in previous work [27]. From the results in Fig. 2 we can conclude that the characteristics of the resonant peaks are changed significantly by including the effects of pressure, concentration, and temperature.

In Fig. 3 we present our results for the FWHM corresponding to the peaks obtained in Fig. 2. Each panel in Fig. 3 has the same parameters as the corresponding panel in Fig. 2. The P-dependent FWHM is shown in Fig. 3(a). Unlike in the previous works [45,46,57], where only the phonon emission process is studied, the results in present study cover all possible processes: both phonon absorption and emission as well as both one- and two-photon. In all four cases, the FWHM dresses as a monotonically decreasing function of pressure. This reveals that when the pressure increases the electron-phonon interaction decreases. This result comes from the fact that with the increase of the pressure the well-shape becomes broader, leading to the reduction of the quantum confinement effect, and so does the electron–phonon interaction. Since till $P = 30$ kbar the size of quantum wells changes less than 1%, the size of the quantum well does not depend on the hydrostatic pressure, therefore, in this work, we are not considering the fractional change of the volume with the hydrostatic pressure.

The P-dependent FWHM can be quantitatively analysed by using a fitted expression as follows

$$\mathrm{FWHM}(P) = \alpha_P + \beta_P P + \gamma_P P^2, \tag{28}$$

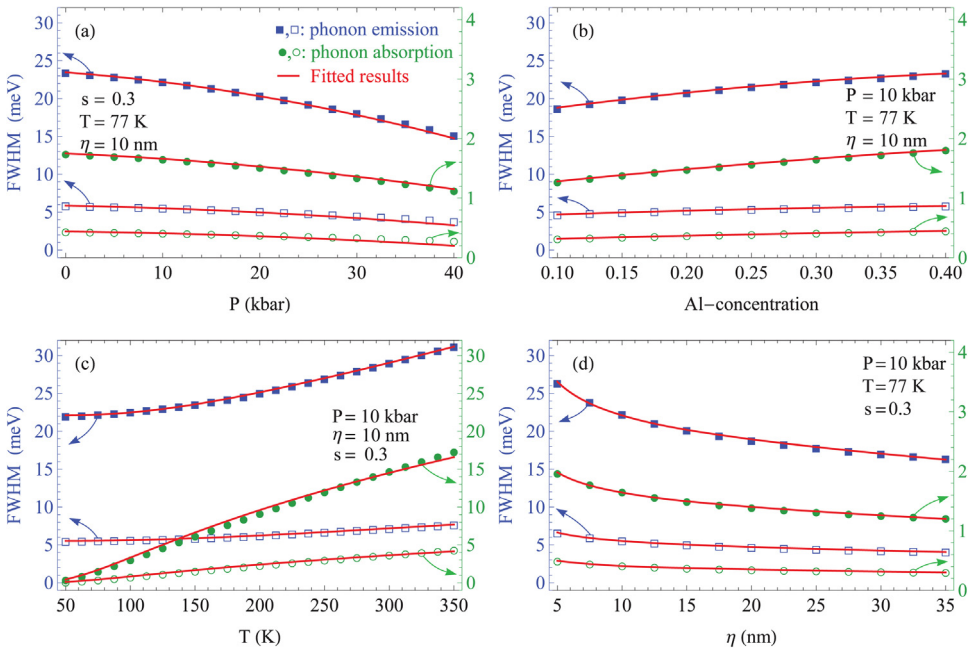

Fig. 3. Dependence of FWHM on hydrostatic pressure (a), Al-concentration (b), temperature (d), and η-parameter (d). The full and empty symbols, respectively, refer to the one- and two-photon resonances. Squares and circles are for phonon emission and absorption, respectively.

where α_P, β_P, and γ_P are the fitted parameters obtained from a fit of the FWHM to each line in Fig. 3(a) using Eq. (28). The result of these fitted parameters is indicated in the Table 1, and the fitted results from Eq. (28) are displayed by the red solid curves in Fig. 3(a). The perfect fit between them means that the nonlinear fit in Eq. (28) is a good expression to describe the dependence of the FWHM on the pressure. Although there is currently no experimental data to support this prediction, we hope that this result would be verified by an experimental study in the future.

Besides the cause of the reduction in the intensity and the blue-shift behavior of the absorption peak, the increase of concentration is also the cause of the enhancement of the FWHM. Fig. 3(b) displays the dependence of the FWHM on the concentration for altogether four processes. It is observed that the FWHM increases with the concentration for all processes. This implies that the higher concentration is the stronger the electron-phonon interaction is. In addition, we can see that the values of FWHM in the present work is bigger than those in other types of quantum well [45,46,57]. To have a more accurate result we suggest an analytic expression describing the concentration dependence of the FWHM as follows

$$\mathrm{FWHM}(s) = \alpha_s + \beta_s s + \gamma_s s^2, \tag{29}$$

where α_s, β_s, and γ_s are the fitted parameters whose values are listed in the Tab. 1 . A fitting result is illustrated by the solid lines in Fig. 3(b). The good fit between them shows that Eq. (29) is a sufficient expression to describe the dependence of the FWHM on the concentration and it is needed to test by experimental work in the future.

In Fig. 3(c), we depict the temperature dependent FWHM for all four processes. The FWHM is observed to increase with the increase in temperature but with different rules for different phonon processes. In the case of phonon emission, the FWHM is proportional to N_ω while a $N_\omega^{1/2}$-dependent rule of the FWHM is found in the case of phonon absorption. It can be seen from Fig. 3(c), FWHM broadens monotonously with the increase of temperature, which can be frequently described using the following expression

$$\mathrm{FWHM}(T) = \alpha_T + \beta_T N_\omega, \tag{30}$$

where the fitted parameters α_T and β_T stand for the balanced and thermal broadening parts of FWHM, respectively [59–61]. In the

Table 1
The fitted results of parameters α_i, β_i and γ_i ($i = P, s$).

Parameters	Line ■	Line □	Line ●	Line ○
α_P (meV)	23.47	5.86	1.75	0.44
β_P (meV kbar^{-1})	−0.098	−0.025	−0.007	−0.002
γ_P (meV kbar^{-2})	−0.003	−0.001	−0.0002	−0.0001
α_s (meV)	16.33	4.07	1.05	0.26
β_s (meV)	27.09	6.78	2.45	0.61
γ_s (meV)	−24.10	−6.04	−1.37	−0.34

Table 2
The fitted results of parameters α_i, β_i and γ_i ($i = T, \eta$).

Parameters	Line ■	Line □	Line ●	Line ○
α_T (meV)	22.11	5.53	–	–
β_T (meV)	19.29	4.58	–	–
γ_T (meV)	–	–	24.20	6.05
α_η (meV)	19.48	4.86	1.44	0.36
β_η (meV nm^{-1})	−0.12	−0.03	−0.01	−0.002
γ_η (meV nm)	38.41	9.63	2.93	0.74

case of phonon absorption, the corresponding expression is $\mathrm{FWHM}(T) = \gamma_T N_\omega^{1/2}$. The fitted results for α_T, β_T, and γ_T are listed in Table 2 and performed in Fig. 3(c) by the red solid curves, which fit well with the FWHM data obtained from the numerical calculations (square and circle dots). The obtained values here of the fitted parameters are changed completely in comparison with those reported in the previous work [27] where the effects of the pressure and the concentration are neglected. While stable parts, α_T, here are somewhat smaller, the thermal broadening parts, β_T, are larger than those of previous work [27]. This complex result comes from the opposite effect of the pressure and the concentration: while the increase of the pressure results in a decrease of the FWHM [see Fig. 3(a)], the enhanced concentration is the cause of a reverse trend of the FWHM [see Fig. 3(b)].

Finally, the variation of the FWHM with the η-parameter for certain values of P, T, and s is presented in Fig. 3(d). The FWHM is found to decrease with the increase of the η-parameter, being in agreement with previous finding [27]. Since the η-parameter stands for the quantum well-width, the reduction of the FWHM means that the probability of electron-phonon interaction decreases with the well-width. The η-dependent FWHM can be read

$$\mathrm{FWHM}(\eta) = \alpha_\eta + \beta_\eta \eta + \gamma_\eta \eta^{-1}, \tag{31}$$

where the η-parameter is measured in the unit of nm, α_η, β_η, and γ_η are the fitted parameters. The fitted results in Eq. (31) with the fitted parameters listed in Table 2 are presented in Fig. 3(d) by the red solid curves. We can see that Eq. (31) is a good expression to describe the η-dependence of the FWHM. Unfortunately, there are currently not any experimental data to support this suggestion. We hope that this result would be verified in the near future.

4. Conclusion

We have discussed theoretically the effects of the hydrostatic pressure, Al-concentration, and temperature on the MOAPs of the HTQW by studying the MOAC and the FWHM. Our results cover four possible processes: both phonon absorption and emission as well as both one- and two-photon. The results showed that the MOAPs of the HTQW significantly depend on the hydrostatic pressure, the Al-concentration, the temperature, and the η-parameter. (i) The increased pressure leads to the decrease of the energy separation, the red-shift behavior of the MOAC peaks, and the reduction of the FWHM. (ii) When the Al-concentration increases, the energy separation increases, the MOAC peaks show a blue-shift and a reduction in the intensity, and the FWHM is enhanced. (iii) The increased temperature results in the slight enhancement of the energy separation, leading to a slight blue-shift of the MOAC peaks, and the increase of the FWHM. The influence of the temperature on the resonant peak intensity is non-monotonic: lower temperature values induce a reduction while for higher temperature values the peak intensity is enhanced. (iv) The increase of the η-parameter leads to the red-shift of the MOAC peaks and the drop of the FWHM.

We also found that the phonon emission process occurs stronger than that of the phonon absorption especially in the range of lower temperatures. At the room-temperature, the phonon absorption process is still weaker but almost asymptotic to the emission one. In both cases of phonon processes, the two-photon absorption is always weaker but comparable with the one-photon absorption. In addition, we also found two analytical expressions for the dependence of the FWHM on the hydrostatic pressure and the Al-concentration as shown in Eqs. (28) and (29). These results are new and need an experimental study to examine their validity in the future.

Acknowledgments

This work is funded by Ministry of Education and Training (Vietnam) under the project coded B2018.PSD.01. C.A. Duque is grateful to the Colombian Agencies: CODI-Universidad de Antioquia (Estrategia de Sostenibilidad de la Universidad de Antioquia and projects “Efectos de capas delta dopadas en pozos cuánticos como fotodetectores en el infrarrojo”, “Propiedades magneto-ópticas y óptica no lineal en superredes de Grafeno”, “Efectos ópticos intersubbanda, no lineales de segundo orden y dispersión Raman, en sistemas asimétricos de pozos cuánticos acoplados” and “Estudio de propiedades ópticas en sistemas semiconductores de dimensiones nanoscópicas”) and Facultad de Ciencias Exactas y Naturales-Universidad de Antioquia (CAD-exclusive dedication project 2018-2019).

References

[1] E. Leobandung, L. Guo, S.Y. Chou, Appl. Phys. Lett. 67 (1995) 2338.

[2] J. Faist, F. Capasso, D.L. Sivco, C. Sirtori, A.L. Hutchinson, A.Y. Cho, Science 264 (1994) 553.
[3] D.M.-T. Kuo, A. Fang, Y.C. Chang, Infrared Phys. Technol. 42 (2001) 433.
[4] X. Liu, N. Li, W. Lu, N. Li, X. Yuan, S. Shen, L. Fu, H. Tan, C. Jagadish, Jpn. J. Appl. Phys. 39 (2000) 1687.
[5] A. Kirilyuk, T. Rasing, R. Mégy, P. Beauvillain, Phys. Rev. Lett. 77 (1996) 4608.
[6] I. Karabulut, S. Baskoutas, J. Appl. Phys. 103 (2008) 073512.
[7] K. Batra, V. Prasad, Eur. Phys. J. B 91 (2018) 298.
[8] K. Guo, G. Liu, L. Huang, X. Zheng, Opt. Mater. 46 (2015) 361.
[9] H.M. Baghramyan, M.G. Barseghyan, A.A. Kirakosyan, R.L. Restrepo, M.E. Mora-Ramos, C.A. Duque, J. Lumin. 145 (2014) 676.
[10] H. Dakhlaoui, J. Appl. Phys. 117 (2015) 135705.
[11] L.M. Burileanu, A. Radu, Opt. Commun. 284 (2011) 2050.
[12] H. Yıldırım, M. Tomak, Phys. Rev. B 72 (2005) 115340.
[13] I. Karabulut, U. Atav, H. Şafak, M. Tomak, Eur. Phys. J. B 55 (2007) 283.
[14] F. Ungan, J.C. Martínez-Orozco, R.L. Restrepo, M.E. Mora-Ramos, E. Kasapoglu, C.A. Duque, Superlattices Microstruct. 81 (2015) 26.
[15] J.H. Bechtel, W.L. Smith, Phys. Rev. B 13 (1976) 3515.
[16] M. Rumi, J.W. Perry, Adv. Opt. Photon. 2 (2010) 451.
[17] A. Shimizu, T. Ogawa, H. Sakaki, Phys. Rev. B 45 (1992) 11338.
[18] L.A. Padilha, G. Nootz, P.D. Olszak, S. Webster, D.J. Hagan, E.W. Van Stryland, L. Levina, V. Sukhovatkin, L. Brzozowski, E.H. Sargent, Nano Lett. 11 (2011) 1227.
[19] K. Wei, Z. Xu, R. Chen, X. Zheng, X. Cheng, T. Jiang, Opt. Lett. 41 (2016) 3821.
[20] H.N. Spector, Phys. Rev. B 35 (1987) 5876.
[21] D. More, C. Rajesh, A.D. Lad, G.R. Kumar, S. Mahamuni, Opt. Commun. 283 (2010) 2150.
[22] V. Dneprovskii, M. Kozlova, A. Smirnov, T. Wumaier, Physica E 44 (2012) 1920.
[23] P. Dharmaraj, K. Jeganathan, V. Gokulakrishnan, P.S. Venkatesh, R. Parameshwari, V. Ramakrishnan, S. Balakumar, K. Asokan, K. Ramamurthi, J. Phys. Chem. C 117 (2013) 19195.
[24] G.L. Dakovski, J. Shan, J. Appl. Phys. 114 (2013) 014301.
[25] J. Khatei, C.S. Suchand Sandeep, R. Philip, K.S.R. Koteswara Rao, Appl. Phys. Lett. 100 (2012) 081901.
[26] Z. Wang, Physica E 43 (2011) 1329.
[27] K.D. Pham, L. Dinh, P.T. Vinh, C.A. Duque, H.V. Phuc, C.V. Nguyen, Superlattices Microstruct. 120 (2018) 738.
[28] E. Ozturk, I. Sökmen, Opt. Commun. 285 (2012) 5223.
[29] B. Welber, M. Cardona, C.K. Kim, S. Rodriguez, Phys. Rev. B 12 (1975) 5729.
[30] D.E. Aspnes, Phys. Rev. B 14 (1976) 5331.
[31] E. Reyes-Gómez, N. Raigoza, L.E. Oliveira, Phys. Rev. B 77 (2008) 115308.
[32] I.A. Yugova, A. Greilich, D.R. Yakovlev, A.A. Kiselev, M. Bayer, V.V. Petrov, Y.K. Dolgikh, D. Reuter, A.D. Wieck, Phys. Rev. B 75 (2007) 245302.
[33] H.M. Baghramyan, M.G. Barseghyan, A.A. Kirakosyan, R.L. Restrepo, C.A. Duque, J. Lumin. 134 (2013) 594.
[34] S. Adachi, J. Appl. Phys. 58 (1985) R1.
[35] G.A. Samara, Phys. Rev. B 27 (1983) 3494.
[36] M. Karimi, G. Rezaei, M. Nazari, J. Lumin. 145 (2014) 55.
[37] M. Nazari, M.J. Karimi, A. Keshavarz, Physica B 428 (2013) 30.
[38] E. Kasapoglu, Phys. Lett. A 373 (2008) 140.
[39] I. Erdogan, O. Akankan, H. Akbas, Superlattices Microstruct. 59 (2013) 13.
[40] A.M. Elabsy, J. Phys.: Condens. Matter 6 (1994) 10025.
[41] M.E. Mora-Ramos, S.Y. López, C.A. Duque, Eur. Phys. J. B 62 (2008) 257.
[42] M.E. Mora-Ramos, S.Y. López, C.A. Duque, Physica E 40 (2008) 1212.
[43] L. Lu, W. Xie, Z. Shu, Physica B 406 (2011) 3735.
[44] F. Ungan, U. Yesilgul, S. Sakiroglu, M.E. Mora-Ramos, C.A. Duque, E. Kasapoglu, H. Sari, I. Sökmen, Opt. Commun. 309 (2013) 158.
[45] H.V. Phuc, J. Phys. Chem. Solids 82 (2015) 36.
[46] T.C. Phong, H.V. Phuc, Superlattices Microstruct. 83 (2015) 755.
[47] I.I. Gol'dman, V.D. Krivchenkov, V.I. Kogan, V.M. Galitskii, Problems in Quantum Mechanics, Inforsearch, London, 1960.
[48] W. Guang-Hui, G. Kang-Xian, G. Qi, Commun. Theor. Phys. 39 (2003) 377.
[49] J.S. Bhat, R.A. Nesargi, B.G. Mulimani, Phys. Rev. B 73 (2006) 235351.
[50] C.V. Nguyen, N.N. Hieu, N.A. Poklonski, V.V. Ilyasov, L. Dinh, T.C. Phong, L.V. Tung, H.V. Phuc, Phys. Rev. B 96 (2017) 125411.
[51] K. Seeger, Semiconductor Physics: An Introduction vol. 40, Springer-Verlag, Berlin Heidelberg, 1985.
[52] W. Xu, R.A. Lewis, P.M. Koenraad, C.J.G.M. Langerak, J. Phys.: Condens. Matter 16 (2004) 89.
[53] W. Xu, Phys. Rev. B 57 (1998) 12939.
[54] J.S. Bhat, S.S. Kubakaddi, B.G. Mulimani, J. Appl. Phys. 70 (1991) 2216.
[55] S.L. Chuang, Physics of Optoelectronic Devices, Wiley, New York, 1995.
[56] E. Li, Physica E 5 (2000) 215.
[57] L. Dinh, H.V. Phuc, Superlattices Microstruct. 86 (2015) 111.
[58] K.D. Pham, N.N. Hieu, L.T.T. Phuong, B.D. Hoi, C.V. Nguyen, H.V. Phuc, Appl. Phys. A 124 (2018) 656.
[59] D.A.B. Miller, D.S. Chemla, D.J. Eilenberger, P.W. Smith, A.C. Gossard, W.T. Tsang, Appl. Phys. Lett. 41 (1982) 679.
[60] J. Lee, E.S. Koteles, M.O. Vassell, Phys. Rev. B 33 (1986) 5512.
[61] D. Gammon, S. Rudin, T.L. Reinecke, D.S. Katzer, C.S. Kyono, Phys. Rev. B 51 (1995) 16785.